 CMES, vol.8, no.2, pp.165-176, 2005

Dynamic Simulation of Long Flexible Fibers in Shear Flow

Wenzhong Tang[1] **and Suresh G. Advani**[1]

Abstract: An optimization method is proposed to simulate the motion of long flexible fibers in shear flow. The fiber is modeled as spheres connected by massless rigid rods and ball-socket joints. The optimization method is mathematically justified and used to obtain the position of a fiber at the next time step from its current position. Results for a single fiber in simple shear flow agree well with those reported in the literature. The usefulness of the method is demonstrated by simulating the motion of two interactive fibers subjected to shear flow field, and by studying the viscosity of dilute suspensions of flexible fibers.

keyword: Optimization method, flexible fiber, shear flow, viscosity.

1 Introduction

Fibers immersed in a fluid occur in a variety of biological and engineering processes [Papanastasiou and Alexandrou (1987), Ramazani, Ait-Kadi, and Grmela (1997), Grigelmo-Miguel, Ibarz-Ribas, and Martín-Belloso (1999), Tornberg and Shelley (2004)]. For example, in composites industry fibers are mixed with polymer resin and the suspension is injected into a mold or extruded through a die to form useful products. Addition of fibers to the polymer matrix results in better physical and mechanical properties. Similar is the case for manufacturing of paper in which one usually deals with natural fibers. During manufacturing of such fiber reinforced composites, it is important to understand and characterize the bulk flow of fiber suspensions. Fiber orientation and spatial distribution in the suspension determine not only its rheological properties, but also the microstructure of the final product, which characterizes its mechanical, thermal, and electrical properties. Therefore, there is need to study fiber dynamics in flow. Considerable benefit can be gained by maximizing fiber length, since a longer fiber with a larger aspect ratio can contribute significantly to composite strength than its short fiber counterpart [McClelland and Gibson (1990), Bartus and Vaidya (2005)]. However, larger the aspect ratio of a fiber, more flexible the fiber will be.

The dynamics of flexible fibers in a flowing suspension has been of scientific interest for nearly three decades. With the assumption of inextensibility and perfect flexibility, Hinch (1976) studied the distortion of a thread in shear flow using slender-body theory. The result was that the distorted thread in simple shear flow became straight and aligned along the flow direction. Yamamoto and Matsuoka (1993) proposed a fiber model of bonded spheres that can stretch, bend and twist, and investigated the motion in shear flow of a flexible fiber with an aspect ratio of up to 20. Ross and Klingenberg (1997) modeled a flexible fiber as a chain of prolate spheroids connected through ball and socket joints. An ideal flexible fiber with an aspect ratio of 25 in shear flow was studied. Joung, Phan-Thien, and Fan (2001) described a flexible fiber as a chain of spherical beads linked by connectors, within each bead being a joint allowing limited bending and torsion. They investigated the distortion of a flexible fiber in shear flow for an aspect ratio of 16.9. Suspension viscosity was calculated using fiber orientation tensors by assuming all fibers remain nearly straight at all times. While most previous studies on the dynamics of flexible fibers paid attention to an aspect ratio of the order of 20, fibers of much larger aspect ratios have been used in fiber reinforced composites. McClelland and Gibson (1990) reported an injection molded nylon 66 composites containing long glass fibers with an aspect ratio of 364. In recent years, there has been a flurry of research focused on the manufacturing of nanotube reinforced polymer composites [Andrews, Jacques, Minot, and Rantell (2002), Tang, Santare, and Advani (2003), Gojny, Wichmann, Köpke, Fiedler, and Schulte (2004)]. The single- or multi-walled nanotubes used usually have aspect ratios as large as 1000. In such cases of large fiber aspect ratios ranging from a few hundred to over one thousand, the

[1] Department of Mechanical Engineering and Center for Composite materials, University of Delaware, Newark, DE 19716-3140, USA

fibers are expected to behave more like a flexible thread rather than a semi-rigid rod. Therefore, external and internal forces in a fiber dominate its motion and deformation but little moment is expected to transfer from one to another part of a fiber. In this paper, our goal is to study the dynamics of long flexible fibers in simple shear flow.

The next section explains our mathematical model and then introduces our optimization method to advance the fiber configuration to the next time step. Mathematical justification is provided for our technique to advance the fiber. Validation of the method is presented by comparing our results with published work and versatility of the method is demonstrated by simulating dynamics of interactive fibers in shear flow.

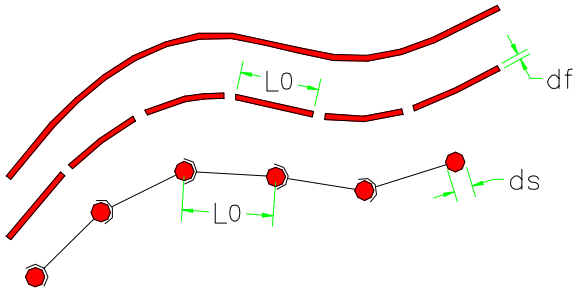

Figure 1 : Sphere-Chain model of a flexible fiber.

2 Flexible fiber model

2.1 *Physical model of a flexible fiber*

To simulate the motion of flexible fiber, we model the fiber as a chain of spheres illustrated in Figure 1. This model is based on the rigid body-hinge model by Skjetne, Ross and Klingenberg (1997) and the chain-of-beads model by Joung, Phan-Thien and Fan (2001). In our model, a continuous fiber of length L_f and diameter d_f is discretized into a number of small segments of length L_0; next the segments are lumped into individual spheres of diameter d_s , the volume of which is the same as that of the corresponding segments; finally the spheres are connected by rigid massless rods of length L_0 to maintain constant fiber length, and ball-socket joints are used to allow free rotation between neighboring segments. The interaction between the fiber and the suspending fluid and between the fibers is through the spheres. There are two types of forces acting on each sphere: external forces and internal forces. External forces include viscous drag from the moving fluid and short-range lubrication forces when two spheres are in close proximity. Viscous drag on each sphere is calculated from the drag on the corresponding fiber segments. The orientation of the ith segment R_i is taken as the direction from the $(i-1)$th sphere to the $(i+1)$th sphere (Figure 2). Considering a circular cylinder in a uniform unbounded flow at low Reynolds numbers, the Stokes drag per unit length on a fiber segment in the transverse direction $\mathrm{F}_{\mathrm{d}_\perp}$ is calculated as [Happel and Brenner (1973), Lamb (1993)]

$$\mathrm{F}_{\mathrm{d}_\perp} = \frac{4\pi\mu\,\mathrm{du}_\perp}{1/2-\gamma-\ln(\rho_f r_f \mathrm{du}_\perp/4\mu)} \tag{1}$$

where μ is the viscosity of the suspending fluid, $\mathrm{du}_\perp$ is the relative velocity of the moving fluid to the fiber segment at its centroid in the transverse direction, $\gamma = 0.577$ is Euler's constant, ρ_f is the density of the fluid and r_f is the radius of the fiber. In this work, the fluid viscosity of $\mu = 1\times10^{-3}\ Pa\cdot s$, and the density of the fluid equal to $\rho_f = 1000\ kg/m^3$ were used. Taking into account the axial motion of a circular cylinder of finite length in a fluid of infinite extent at low Reynolds numbers, the Stokes drag per unit length on a segment in the axial direction is calculated as [Broersma (1960), Cox (1970)]

$$\mathrm{F}_{\mathrm{d}_\parallel} = \frac{2\pi\mu\,\mathrm{du}_\parallel}{\ln(Lf/rf)-0.80685} \tag{2}$$

where $\mathrm{du}_\parallel$ is the relative velocity of the fluid with respect to the segment centroid in the axial direction.

The lubrication force exists when the gap between two spheres approaching each other is less than $0.1ds$ (10% of their diameters, see Figure 3). It is calculated using the following equation [Kim and Karilla (1991), Joung, Phan-Thien and Fan (2001)]

$$\mathrm{F}_{ij} = -\,3\pi\mu\frac{(ds/2)^2}{gap}\mathrm{V}_{sqz} \tag{3}$$

where the relative squeezing velocity V_{sqz} along the centerline between the two spheres can be expressed as

$$\mathrm{V}_{sqz} = \frac{\mathrm{r}_{ij}}{|\mathrm{r}_{ij}|}\left[\frac{\mathrm{r}_{ij}}{|\mathrm{r}_{ij}|}\bullet(\mathrm{V}_j-\mathrm{V}_i)\right]. \tag{4}$$

where $\mathrm{r}_{ij} = \mathrm{r}_j - \mathrm{r}_i$ is the position vector from sphere i to sphere j, and V_i and V_j are their velocities respectively.

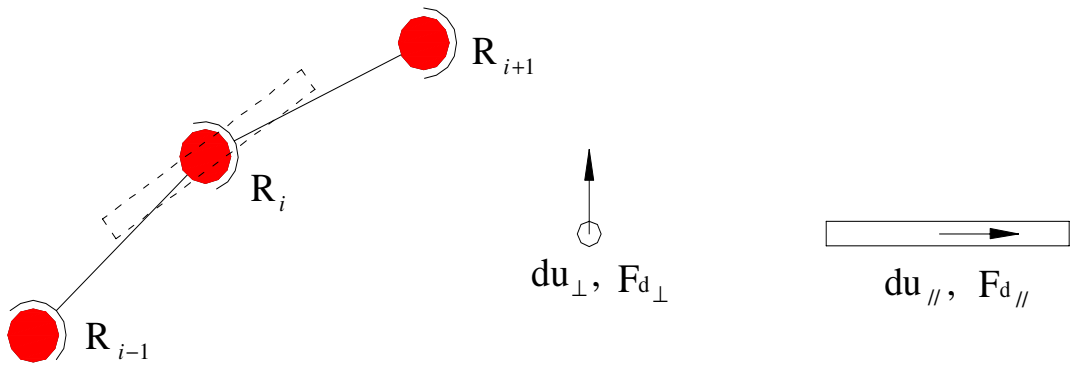

(a) Segment orientation; (b) Transverse drag; (c) Parallel drag

Figure 2 : Stokes drag on a fiber segment.

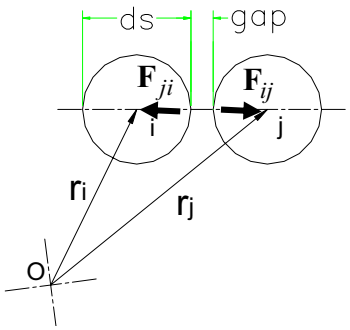

Figure 3 : Lubrication force between two spheres in close proximity.

The internal forces are between neighboring spheres of the same fiber and along the direction of their connective rod, which will be illustrated in Figure 5.

2.2 *Use of minimizing principle to track fiber movement*

Minimal principles in physics have been sought for more than two thousand years [Marion (1970)]. When a physical process takes place, nature always acts in such a way that certain important quantities are minimized. In this work, our method is based on such a notion of minimal principle.

Given current positions and velocities of fibers and velocity field of the flow, the drag force and lubrication forces acting on each sphere are calculated. Figure 4a shows, at current time step, a fiber consisting of spheres at different positions R_i^t, velocities V_i^t, and external forces F_i^t $(i = 1, 2, \cdots, n)$. To obtain the new position of a fiber at the next time step, first the constraints between neighboring spheres are removed (Figure 4b), enabling each sphere to move independently, which leads to a set of pseudo new sphere positions $\overline{R}_i^{t+1}$ (Figure 4c). Let R_i^{t+1} be the actual new positions of the spheres (Figure 4d). Intuitively the actual new positions R_i^{t+1} of a fiber can be derived from these pseudo new positions $\overline{R}_i^{t+1}$. Let $d_i = \left|\mathrm{R}_i^{t+1} - \overline{R}_i^{t+1}\right|$ be the distance between the pseudo and the actual new positions of the ith sphere in the fiber. Inspired by the minimal principles, we seek the actual new positions by minimizing the sum of square of d_i, that is,

$$\min \sum_{i=1}^{n} d_i^2 \tag{5}$$

Also the fibers were assumed to be inextensible. The constraints are

$$\left|\mathrm{R}_{i+1}^{t+1} - \mathrm{R}_i^{t+1}\right| = L_0,\ i = 1, 2, \cdots, n-1 \tag{6}$$

where L_0 is the length of each segment. Therefore, the mathematical model is in principle a typical optimization problem.

3 Justification of the mathematical model

In this section, the proposed optimization method is justified using particle dynamics. It will be shown that the

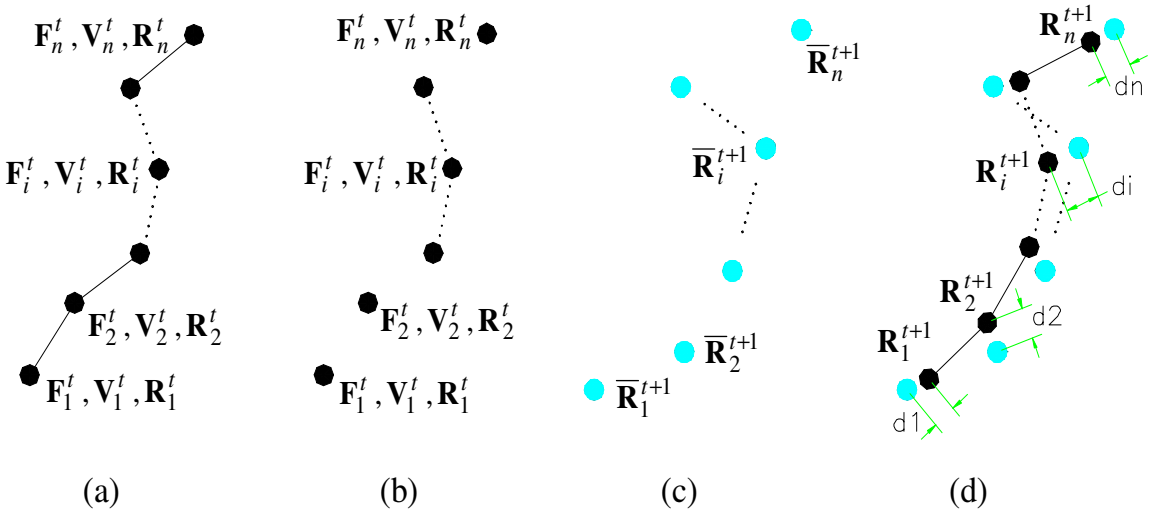

Figure 4 : Mathematical model for obtaining new fiber position. a- Current position; b- Uncoupled spheres; c- Pseudo new position; d- Actual new position.

two methods yield the same result.

3.1 Optimization method

Refer to Figure 4, the pseudo new positions of the spheres are calculated as,

$$\begin{cases} \overline{R}_1^{t+1} = \mathrm{R}_1^t + \mathrm{v}_1^t \Delta t + \frac{\mathrm{F}_1^t}{2m}(\Delta t)^2 \\ \overline{R}_2^{t+1} = \mathrm{R}_2^t + \mathrm{v}_2^t \Delta t + \frac{\mathrm{F}_2^t}{2m}(\Delta t)^2 \\ \quad \vdots \\ \overline{R}_i^{t+1} = \mathrm{R}_i^t + \mathrm{v}_i^t \Delta t + \frac{\mathrm{F}_i^t}{2m}(\Delta t)^2 \\ \quad \vdots \\ \overline{R}_n^{t+1} = \mathrm{R}_n^t + \mathrm{v}_n^t \Delta t + \frac{\mathrm{F}_n^t}{2m}(\Delta t)^2 \end{cases} \tag{7}$$

where Δt is the time interval from current time step to the next time step, and m is the mass of each sphere. To obtain the actual new positions of the spheres, the optimization problem is formulated as,

Minimize

$$\sum_{i=1}^{n} (\mathrm{R}_i^{t+1} - \overline{R}_i^{t+1})^2 \tag{8}$$

subjected to

$$(\mathrm{R}_{i+1}^{t+1} - \mathrm{R}_i^{t+1})^2 = d^2,\ i = 1,\ 2,\ \cdots,\ n-1 \tag{9}$$

To solve the above optimization problem, the following equations are derived using Lagrange Multiplier method [Greenberg (1988)],

$$\begin{cases} (\mathrm{R}_1^{t+1} - \overline{R}_1^{t+1}) + \lambda_1(\mathrm{R}_1^{t+1} - \mathrm{R}_2^{t+1}) = 0 \\ (\mathrm{R}_2^{t+1} - \overline{R}_2^{t+1}) - \lambda_1(\mathrm{R}_1^{t+1} - \mathrm{R}_2^{t+1}) \\ \qquad\qquad + \lambda_2(\mathrm{R}_2^{t+1} - \mathrm{R}_3^{t+1}) = 0 \\ \quad \vdots \\ (\mathrm{R}_i^{t+1} - \overline{R}_i^{t+1}) - \lambda_{i-1}(\mathrm{R}_{i-1}^{t+1} - \mathrm{R}_i^{t+1}) \\ \qquad\qquad + \lambda_i(\mathrm{R}_i^{t+1} - \mathrm{R}_{i+1}^{t+1}) = 0 \\ \quad \vdots \\ (\mathrm{R}_n^{t+1} - \overline{R}_n^{t+1}) - \lambda_{n-1}(\mathrm{R}_{n-1}^{t+1} - \mathrm{R}_n^{t+1}) = 0 \end{cases} \tag{10}$$

where λ_i ($i = 1,\ 2,\ \cdots,\ n-1$) are unknown multipliers. Thus, the total number of unknowns are 4n-1, 3n for R_i^{t+1} ($i = 1,\ 2,\ \cdots,\ n$, three components for each sphere) and n-1 for λ_i ($i = 1,\ 2,\ \cdots,\ n-1$). We have exactly the same number of equations from Equations 9 and 10. These nonlinear equations can be solved using Newton's iterative method [Ortega and Rheinboldt (1970)].

3.2 Particle dynamics

The actual new sphere positions R_i^{t+1} at the next time step in Fig 4d can also be obtained directly from their

current new positions R_i^t using particle dynamics. Apart from external forces (drag force and lubrication force), the particles are also subjected to internal forces applied by neighboring spheres on the same fiber. The forces applied on the ith sphere of a fiber are shown in Figure 5.

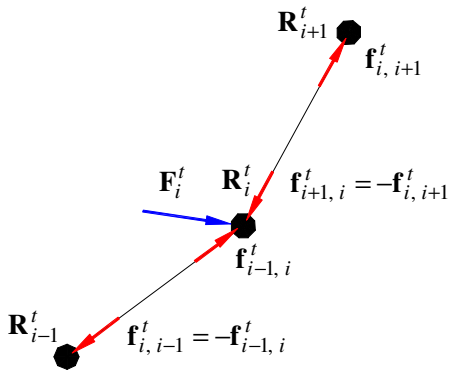

Figure 5 : Forces acting on the ith sphere of a fiber at current time step.

In the above figure, F_i^t is the resultant external force including drag force and lubrication forces, $\mathrm{f}_{i-1,i}^t$ the internal force applied by the $(i-1)$th particle, and $\mathrm{f}_{i+1,i}^t$ the internal force applied by the $(i+1)$th particle. At the next time step, the new positions of the spheres are given by

$$\begin{cases} \mathrm{R}_1^{t+1} = \mathrm{R}_1^t + \mathrm{v}_1^t \Delta t + \dfrac{\mathrm{F}_1^t + \mathrm{f}_{2,1}^t}{2m}(\Delta t)^2 \\ \qquad = \overline{R}_1^{t+1} - \dfrac{\mathrm{f}_{1,2}^t}{2m}(\Delta t)^2 \\ \mathrm{R}_2^{t+1} = \mathrm{R}_2^t + \mathrm{v}_2^t \Delta t + \dfrac{\mathrm{F}_2^t + \mathrm{f}_{1,2}^t + \mathrm{f}_{3,2}^t}{2m}(\Delta t)^2 \\ \qquad = \overline{R}_2^{t+1} + \dfrac{\mathrm{f}_{1,2}^t - \mathrm{f}_{2,3}^t}{2m}(\Delta t)^2 \\ \qquad \vdots \\ \mathrm{R}_i^{t+1} = \mathrm{R}_i^t + \mathrm{v}_i^t \Delta t + \dfrac{\mathrm{F}_i^t + \mathrm{f}_{i-1,i}^t + \mathrm{f}_{i+1,i}^t}{2m}(\Delta t)^2 \\ \qquad = \overline{R}_i^{t+1} + \dfrac{\mathrm{f}_{i-1,i}^t - \mathrm{f}_{i,i+1}^t}{2m}(\Delta t)^2 \\ \qquad \vdots \\ \mathrm{R}_n^{t+1} = \mathrm{R}_n^t + \mathrm{v}_n^t \Delta t + \dfrac{\mathrm{F}_n^t + \mathrm{f}_{n-1,n}^t}{2m}(\Delta t)^2 \\ \qquad = \overline{R}_n^{t+1} + \dfrac{\mathrm{f}_{n-1,n}^t}{2m}(\Delta t)^2 \end{cases} \tag{11}$$

in which Equation 7 was used for simplification. In the above equations, $\mathrm{f}_{i,\,i+1}^t$ $(i = 1,\, 2,\, \cdots,\, n-1)$ takes the direction of the connective rod between the ith and $(i+1)$th spheres. It can be expressed as,

$$\mathrm{f}_{i,\,i+1}^t = c_i(\mathrm{R}_i^t - \mathrm{R}_{i+1}^t), \quad i = 1,\, 2,\, \cdots,\, n-1 \tag{12}$$

where c_i $(i = 1,\, 2,\, \cdots,\, n-1)$ are scalar coefficients. Since the time step Δt is small, we use $(\mathrm{R}_i^{t+1} - \mathrm{R}_{i+1}^{t+1})$ to approximate $(\mathrm{R}_i^t - \mathrm{R}_{i+1}^t)$ in Equation 12. The justification for this approximation are: (i) The spheres displace by a small distance within a small time interval, so the change in the direction of the connective rod, or the difference between $(\mathrm{R}_i^{t+1} - \mathrm{R}_{i+1}^{t+1})$ and $(\mathrm{R}_i^t - \mathrm{R}_{i+1}^t)$ is small; and (ii) When these approximated forces $\mathrm{f}_{i,\,i+1}^t$ are substituted back in Equation 11, they are multiplied by $(\Delta t)^2$, making the approximation errors even smaller. After this approximation Equation 12 becomes

$$\mathrm{f}_{i,\,i+1}^t = c_i(\mathrm{R}_i^{t+1} - \mathrm{R}_{i+1}^{t+1}), \quad i = 1,\, 2,\, \cdots,\, n-1 \tag{13}$$

Substitution of Equation 13 into Equation 11 yields

$$\begin{cases} (\mathrm{R}_1^{t+1}-\overline{R}_1^{t+1})+\mu_1(\mathrm{R}_1^{t+1}-\mathrm{R}_2^{t+1})=0 \\ (\mathrm{R}_2^{t+1}-\overline{R}_2^{t+1})-\mu_1(\mathrm{R}_1^{t+1}-\mathrm{R}_2^{t+1}) \\ \qquad\qquad +\mu_2(\mathrm{R}_2^{t+1}-\mathrm{R}_3^{t+1})=0 \\ \quad \vdots \\ (\mathrm{R}_i^{t+1}-\overline{R}_i^{t+1})-\mu_{i-1}(\mathrm{R}_{i-1}^{t+1}-\mathrm{R}_i^{t+1}) \\ \qquad\qquad +\mu_i(\mathrm{R}_i^{t+1}-\mathrm{R}_{i+1}^{t+1})=0 \\ \quad \vdots \\ (\mathrm{R}_n^{t+1}-\overline{R}_n^{t+1})-\mu_{n-1}(\mathrm{R}_{i-1}^{t+1}-\mathrm{R}_i^{t+1})=0 \end{cases} \tag{14}$$

where $\mu_i=\frac{c_i}{2m}(\Delta t)^2$, $i=1,\ 2,\ \cdots,\ n-1$, are scalar coefficients to be determined. The constraints are same as those in Equation 9. It can be seen that the only difference between Equation 10 and Equation 14 are the symbols for unknown coefficients. If we change μ_i in Equation 14 into λ_i, then the two sets of equations are identical. Therefore, the two methods, the optimization method and particle dynamics method, give the same results for $\mathrm{R}_i^{t+1}(i=1,\ 2,\ \cdots,\ n)$, the actual positions of the spheres at the next time step.

4 Numerical simulation

The flexible fiber model coupled with the optimization method to advance the fiber to the next time step was used to study single fiber and two fibers in close proximity in shear flows. Also, the viscosities of two dilute flexible fiber suspensions were calculated.

4.1 Single flexible fiber

To verify our method and the simulation of flexible fiber dynamics, the motion and deformation of a single flexible fiber in simple shear flow was investigated. Here we considered two cases: initially s-shaped fiber ($x=430000y^3-2y$, $-0.0024m\le y\le 0.0024m$) and inverse-s-shaped fiber respectively (Figure 6a). The fiber was discretized into 21 segments, and a unit shear rate $\dot{\gamma}=1\,s^{-1}$ and a time step of $\Delta t=0.001$s was used in our simulation. Figure 6 presents our simulation results and compares them to the results of Hinch (1976) and Joung et al. (2001). The fiber positions in the figure correspond to non-dimensional total strain equal to $\dot{\gamma}t=0,\ 1,\ 2,\ 3,\ 4,\ 5$, and 6 respectively. However, the aspect ratios adopted by the three studies are different. While assuming inextensibility and perfect flexibility, Hinch did not introduce dimensional property to his fiber. Joung et al. used an aspect ratio of 16.9. In the current work, the fibers are $1.6\times10^{-4}\,m$ in diameter and have an aspect ratio of 72.8. From Figure 6, it can be seen that our simulation results qualitatively agree well with the other two sets of results. In each case, the fiber under shear becomes straight and aligns along the flow direction with time.

4.2 Two interactive fibers

When there is more than one fiber in the flow field, the fibers may interact with each other when in close proximity. This does not pose any specific problem for our methodology. The interactions between two fibers are calculated through interactive sphere pairs (Figure 3). In current work, the motion and deformation of two folded fibers in simple shear flow was simulated (Figure 7). The fibers are $1.0\times10^{-4}\,m$ in diameter and have an aspect ratio of 96. Initially, both fibers are folded in the middle. A unit shear rate of $\dot{\gamma}=1\,s^{-1}$ was applied in the simulation. To study the effect of segment size on simulation results, three different segment numbers (9, 17 and 33) were used. The motion and deformation of the two fibers are shown in Figure 7. Under the forces applied by the flow field and the interactive forces between the two fibers, while rotating, the fibers slide against each other, open their ends and become aligned along the flow direction. In this case, 17 segments were sufficient enough for the description of the motion and deformation of the fiber.

4.3 Viscosity of dilute Suspension of Flexible Fibers

The rheological properties of fiber suspensions have been studied by many researchers both experimentally and theoretically [Mason (1954), Batchelor (1970A), Barbosa, Ercoli, Bibbó, and Kenny (1994), Yamamota and Matsuoka (1994), Yamane, Kaneda, and Dio (1994), Ramazani, Ait-Kadi, and Grmela (1997), Ross and Klingenberg (1997), Petrie (1999), Petrich, Koch, and Cohen (2000), Pozrikidis (2004)]. Of these studies, most theoretical work has been done for suspensions of rigid fibers in Newtonian liquids. In general, the flow behavior of fiber suspensions depends on fiber aspect ratio, fiber volume fraction, fiber orientation, and fluid properties. In this work, the viscosity of dilute suspensions of flexible fibers in simple shear flow of Newtonian fluid was calcu-

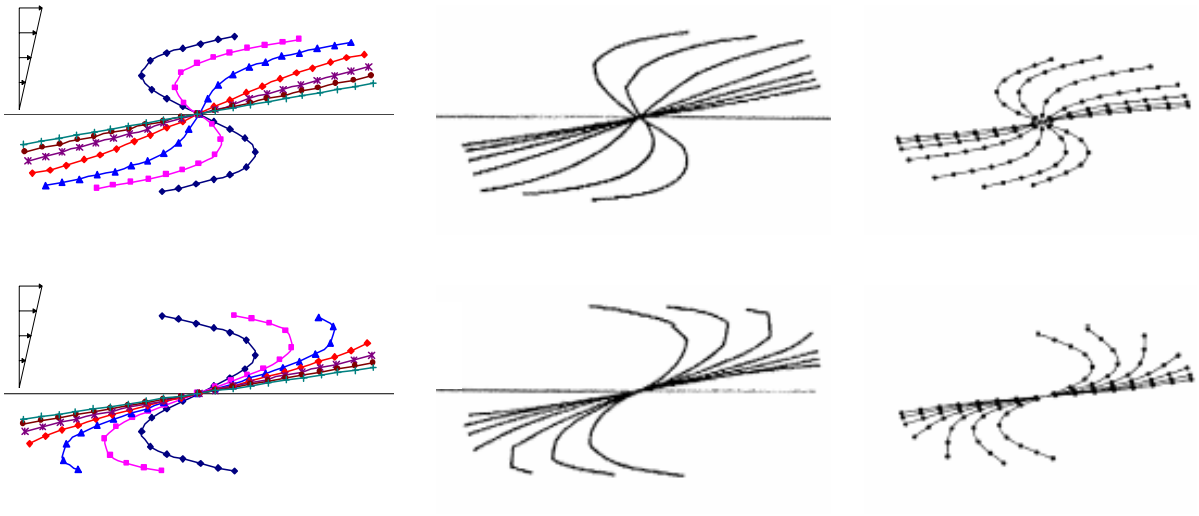

(a) (b) (c)

Figure 6 : Motion of initially s-shaped fiber and inverse-s-shaped fiber in simple shear flow at $\dot{\gamma}t$ =0, 1, 2, 3, 4, 5, 6. (a) Current work; (b) Hinch (1976); (c) Joung et al. (2001).

lated.

One suspension system under investigation is illustrated in Figure 8, where a unit cell with a curved fiber at initial position is presented. The size of the unit cell is $0.008\,m \times 0.005\,m \times 0.001m$ $(x \times y \times z)$. Periodic boundary conditions are applied in all three directions. The fiber is $1.0 \times 10^{-4}\,m$ in diameter. Initially the fiber is assigned an s-shape consisting of two half-circles of radius equal to $1.0 \times 10^{-3}\,m$. The aspect ratio of the fiber is approximately 61.6. The volume fraction of the fiber in the suspension is 0.12%, the flow field is defined as $u(y) = y\,(m/s)$, and the time step used is 0.001s. We limit our calculations to two-dimensional flows, assuming that the fiber motion and deformation only occur in the x-y plane. The rheological properties of a fiber suspension can be described by its effective stress tensor. The bulk stress $\langle \tau_{mn} \rangle$ in the suspension is defined by Batchelor's effective stress tensor [Batchelor (1970B), Ross and Klingenberg (1997)] as

$$\langle \tau_{mn} \rangle = \tau^{\infty}_{mn} + \frac{1}{V} \int_{V0} \tau_{mn} dV \tag{15}$$

where τ^{∞}_{mn} is the stress tensor that would exist in the absence of the fiber; V is the volume of the periodic unit cell; $V0$ is the volume of the fiber; and τ_{mn} is the stress

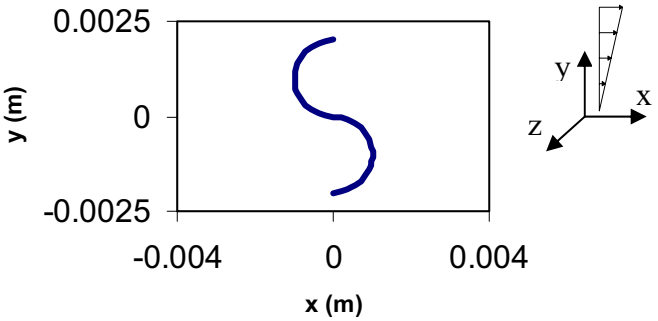

Figure 8 : Unit cell of the curved fiber suspension.

tensor in the fiber with shear stress component [Timoshenko and Goodier (1970)]

$$\tau_{xy} = \sigma \sin\alpha \cos\alpha = \frac{4 f_{i,i+1}}{\pi d_f^2} \sin\alpha \cos\alpha \tag{16}$$

where σ is the normal stress in fiber axis direction, $f_{i,i+1}$ is the internal force in the fiber segment between ith and $(i+1)$th spheres which can be calculated from Equation (11) once the actual new position of the fiber is determined at each time step, and α $(0 \leq \alpha < 2\pi)$ is the angle between the axis of the fiber segment and x axis (Figure 9). The bulk viscosity of the suspension is defined as

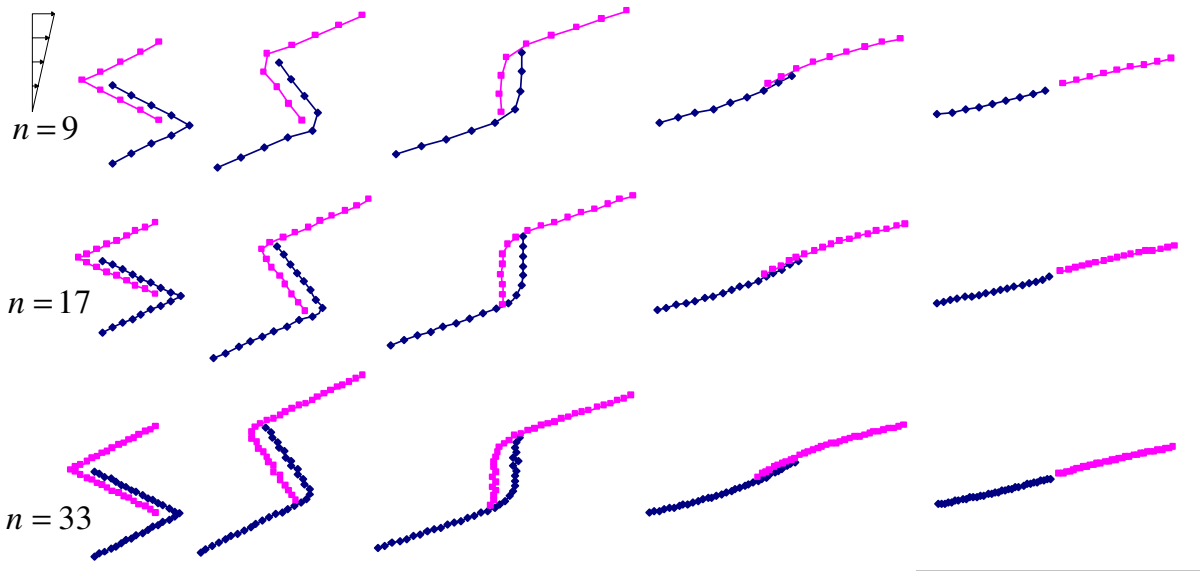

Figure 7 : Configurations of two interactive fibers in simple shear flow at total strain of $\dot{\gamma}t = 0$, 0.5, 1, 2, and 3.

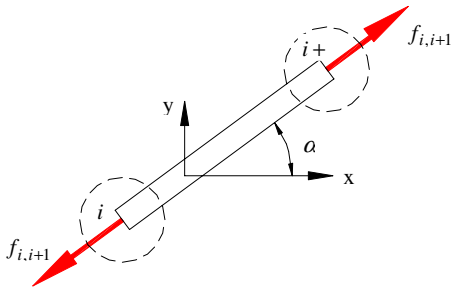

Figure 9 : Internal force contributing to shear stress component in the fiber.

$$\mu_{bulk} = < \tau_{xy} > / \dot{\gamma}_{xy}. \tag{17}$$

where $\dot{\gamma}_{xy}$ is the shear rate in the suspension. Then the relative viscosity of the suspension with respect to fluid viscosity is calculated as

$$\mu_r = \mu_{bulk}/\mu. \tag{18}$$

To verify this method of viscosity calculation, a straight fiber of $4 \times 10^{-3} m$ in length and $2 \times 10^{-4} m$ in diameter was used instead of the curved one in Figure 8. The fiber volume fraction in the suspension was 0.314%. Initially the straight fiber was placed along the y direction in the middle of the unit cell. Figure 9 shows the relative viscosity of the suspension changing with shear value as the fiber changes its orientation. The simulation result is not sensitive to the size of discretized fiber segments. The viscosity reaches its maximum when the fiber forms an angle of 45 degree with the x axis. For comparison, the suspension viscosity was also calculated using the stress equation [Phan-Thien and Graham (1991), Fan, Phan-Thien, and Zheng (1998)] derived from Transversely Isotropic Fluid (TIF) model

$$\begin{aligned} \langle \tau_{ij} \rangle &= 2\mu \mathbf{D}_{ij} \\ &+ \frac{\mu \phi a_r^2}{[\ln(2a_r) - 1.5]} (\mathbf{D} : \text{pppp})_{ij}, \quad 5 < a_r < 30 \end{aligned} \tag{19}$$

and the stress equation [Batchelor (1970A), Sundararajakumar (1997)] from Slender-Body Theory (SBT)

$$\langle \tau_{ij} \rangle = 2\mu \mathbf{D}_{ij} + \frac{2\mu \phi a_r^2}{3\ln(2a_r)} (\mathbf{D} : \text{pppp})_{ij} \tag{20}$$

respectively, where $\mathbf{D}$ is the strain-rate tensor, p is the unit vector parallel to the fiber's axis, ϕ is the volume fraction of the fiber in the suspension, and a_r is the aspect ratio of the fiber. Both equations are based on fiber orientation and for dilute fiber suspensions. It is seen that our result is comparable to, or more exactly, fall in between the results obtained from the above two equations.

In the investigation of the fiber suspension as shown in Figure 8, the fiber is divided into 9, 17, 33 and 65 segments respectively to study the effect of segment size

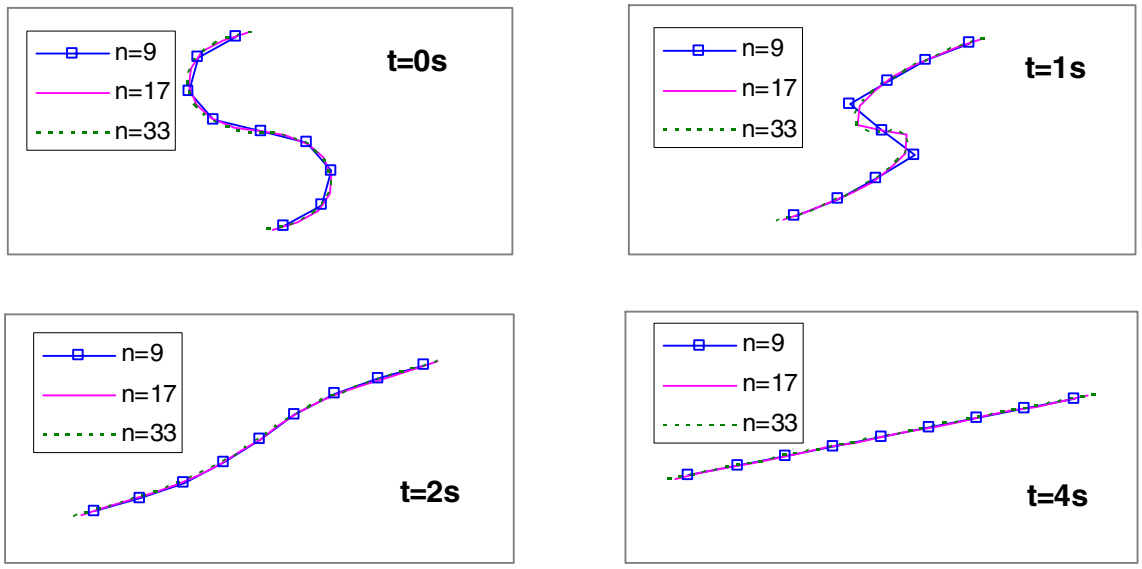

Figure 11 : Fiber configurations at different times.

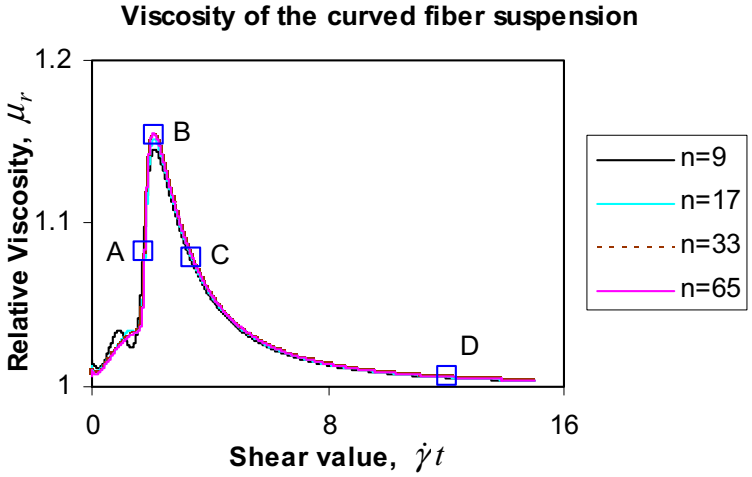

Figure 12 : Relative viscosity of the suspension changes with shear value.

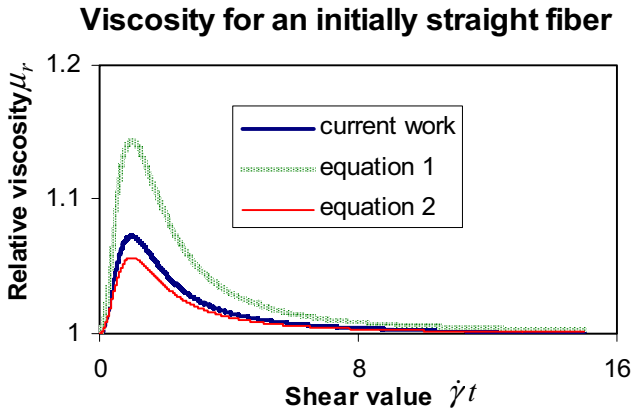

Figure 10 : Viscosity of the suspension containing a straight fiber.

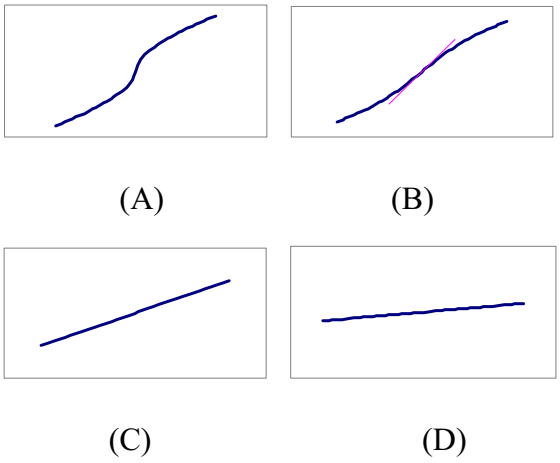

Figure 13 : Fiber configurations corresponding to A, B, C and D in Figure 12.

on the simulation results. Figure 11 shows the configurations of the fiber at different times. The fiber rotates and gradually forms a straight line. It can be seen that 17 segments are sufficient to describe the fiber deformation. The viscosity of the suspension for different segment sizes is shown in Figure 12. As the fiber changes its configuration and orientation, suspension viscosity changes accordingly. In the figure, the curves for 33 and 65 segments coincide with each other, which confirms that the viscosity is convergent with segment size. The convergence of viscosity with the size of time step was also verified in the simulation. The fiber configurations corresponding to configurations A, B, and C in Figure 12 are shown in Figure 13. The relative viscosity of the suspension reaches a maximum of 1.155 when the central part of the fiber forms an angle of about 39 degree with the x axis and approaches unity as the fiber becomes aligned along the flow direction. This viscosity change with fiber configuration in a dilute fiber suspension was also reported by Yamamoto and Matsuoka (1994). In the above suspension system, the fiber density is negligible and no interaction between fibers takes place. If we increase the fiber numbers in the unit cell, semi-concentrated to concentrated suspension-involving interactions between fibers also can be studied.

Conclusions

Long flexible fibers were modeled as sphere-chains linked by rigid rods and ball-socket joints. An optimization method was proposed and mathematically justified for simulating the motion of long flexible fibers in shear flow. Simulation results of an initially s-shaped and inverse-s-shaped fiber in simple shear flow were shown to be in good qualitative agreement with reported results. The motion and deformation of two interactive folded fibers in shear flow were also studied. Results show the two fibers slide against each other and became aligned along the flow field. The principle used in simulation was further applied to study two dilute suspensions containing a flexible fiber. For the suspension containing initially straight fiber, the simulation result is comparable to those obtained using reported methods. For the suspension containing initially curved fiber, the suspension viscosity reaches maximum when the central part of the fiber forms an angle of about 39 degree with flow direction and approaches the viscosity of the suspending fluid as the fiber orientates along the flow direction. The same

method can be used to investigate semi-concentrated to concentrated suspensions of long flexible fibers.

Acknowledgements

This work was financially supported by the National Science Foundation under grant no. DMI-0115127.

References

Andrews, R.; Jacques, D.; Minot, M.; Rantell T. (2002): Fabrication of carbon multiwall nanotube/polymer composites by shear mixing. *Micromolecular Materials and Engineering*, vol. 287, pp. 395-403.

Barbosa, S. E.; Ercoli, D. R.; Bibbó, M. A.; Kenny J. (1994): Rheology of short-fiber composites: A systematic approach. *Composite Structures*, vol. 27, pp. 83-91.

Bartus, S. D.; Vaidya, **U. K.** (2005): Performance of long fiber reinforced thermoplastics subjected to transverse intermediate velocity blunt object impact. *Composite structures*, vol. 67, pp. 263-277.

Batchelor, G. K. (1970A): Slender-body theory for particles of arbitrary cross-section in Stokes flow. *J. Fluid Mech*, vol. 44, pp. 419-440.

Batchelor, G. K. (1970B): The stress system in a suspension of force-free particles. *J. Fluid Mech*, vol. 41, pp. 545-570.

Broersma, S. (1960): Viscous force constant for a closed cylinder. *J. Chem. Phys*, vol. 32, pp. 1632-1635.

Cox, R. B. (1970): The motion of long slender bodies in a viscous fluid Part 1: General theory. *J. Fluid Mech*, vol. 44, pp. 791-810.

Fan, X.; Phan-Thien N.; Zheng R. (1998): A direct simulation of fiber suspensions. *J. Non-Newtonian Fluid Mech*, vol. 74, pp. 113-135.

Gojny, F. H.; Wichmann, M. H. G.; Köpke, U.; Fiedler, B.; Schulte, K. (2004): Carbon nanotube-reinforced epoxy-composites: enhanced stiffness and fracture toughness at low nanotube content. *Composites Sci. Tech*, vol. 64, pp. 2363-2371.

Greenberg, M. D. (1998): Advanced engineering mathematics. Prentice Hall, New Jersey, USA: 665-671.

Grigelmo-Miguel, N.; Ibarz-Ribas, A.; Martín-Belloso, **O.** (1999): Rheology of peach dietary fibre suspensions. *J. Food Engineering*, vol. 39, pp. 91-99.

Happel, J.; Brenner H. (1973): Low Reynolds number hydrodynamics. Noordhoff International Publishing, Leyden, Netherlands: 47-49.

Hinch, E. J. (1976): The distortion of a flexible inextensible thread in a shearing flow. *J. Fluid Mech*, vol. 74, pp. 317-333.

Joung, C. G.; Phan-Thien, N.; Fan, X. J. (2001): Direct simulation of flexible fibers. *J. Non-Newtonian Fluid Mech*, vol. 99, pp. 1-36.

Kim, S.; Karilla, S. J. (1991): Microhydrodynamics: principles and selected applications. Butterworth - Heinemann, Boston, USA: 226-231.

Lamb, S. H. (1993): Hydrodynamics. Dover Publications, New York, USA: 614-617.

Marion, J. B. (1970): Classical Dynamics of Particles and Systems. Academic Press, New York, USA: 197-200.

Mason, S. G. (1954): Fiber motions and flocculation. *Tappi*, vol. 37, pp. 494-501.

McClelland, A. N.; Gibson, A. G. (1990): Rheology and fibre orientation in the injection moulding of long fibre reinforced nylon 66 composites. *Composites manufacturing*, vol. 1, pp. 15-25.

Ortega, J. M.; Rheinboldt, W. C. (1970): Iterative Solution of nonlinear equations in several variables. Academic Press, New York: 181-187.

Papanastasiou, T. C.; Alexandrou, A. N. (1987): Isothermal extrusion of non-dilute fiber suspensions. *J. Non-Newtonian Fluid Mech*, vol. 25, pp. 313-328.

Petrich, M. P.; Koch, D. L.; Cohen, C. (2000): An experimental determination of the stress–microstructure relationship in semi-concentrated fiber suspensions. *J. Non-Newtonian Fluid Mech*, vol. 95, pp. 101-133.

Petrie, C. J. S. (1999): The rheology of fibre suspensions. *J. Non-Newtonian Fluid Mech*, vol. 87, pp. 369-402.

Phan-Thien, N., Graham, A. L. (1991): A new constitutive model for fiber suspensions: flow past a sphere. *Rheol. Acta*, vol. 30, pp. 44-57.

Pozrikidis, C. (2004): Orientation statistics and effective viscosity of suspensions of elongated particles in simple shear flow. *Euro. J. Mech. B/Fluids*, in press.

Ramazani, A.; Ait-Kadi, A.; Grmela, M. (1997): Rheological modeling of short fiber thermoplastic compos-

ites. *J. Non-Newtonian Fluid Mech*. vol. 73, pp. 241-260.

Ross, R. F.; Klingenberg, D. J. (1997): Dynamic simulation of flexible fibers composed of linked rigid bodies. *J. Chem. Phys*, vol. 106, pp. 2949-2960.

Skjetne, P.; Ross, R. F.; Klingenberg, D. J. (1997): Simulation of single fiber dynamics. *J. Chem. Phys*, vol. 107, pp. 2108-2121.

Sundararajakumar, R. R.; Koch, D. L. (1997): Structure and properties of sheared fiber suspensions with mechanical contacts. *J. Chem. Phys*, vol. 73, pp. 205-239.

Tang, W.; Santare, M. H.; Advani, S. G. (2003): Melt processing and mechanical property characterization of multi-walled carbon nanotube/high density polyethylene (MWNT/HDPE) composite films. *Carbon*, vol. 41, pp. 2779-2785.

Timoshenko, S. P.; Goodier, J. N. (1970): Theory of Elasticity. McGRAW-Hill, Singapore: 17-19.

Tornberg, A. K.; Shelley, M. J. (2004): Simulating the dynamics and interactions of flexible fibers in Stokes flows. *J. Computational Phys*, vol. 196, pp. 8-40.

Yamamoto, S.; Matsuoka, T. (1993): A method for dynamic simulation of rigid and flexible fibers in a flow field. *J. Chem. Phys*, vol. 98, pp. 644-650.

Yamamoto, S.; Matsuoka, T. (1994): Viscosity of dilute suspension of rodlike particles: A numerical simulation method. *J. Chem. Phys*, vol. 100, pp. 3317-3324.

Yamane, Y.; Kaneda, Y.; Dio, M. (1994): Numerical simulation of semi-dilute suspensions of rodlike particles in shear flow. *J. Non-Newtonian Fluid Mech*, vol. 54, pp. 405-421.